研究成果の刊行に関する一覧表

書　籍

著者氏名	論文タイトル名	書籍全体の編集者名	書　籍　名	出版社名	出版地	出版年	ページ
加部泰明、末松誠、半田宏		杉浦悠季	実験医学別冊「医学生物学における最新プロトコールと実験例」	羊土社	東京	2014	印刷中

雑　誌

発表者氏名	論文タイトル名	発表誌名	巻号	ページ	出版年
Takenouchi T, Nishina S, Kosaki R, Torii C, Furukawa R, Takahashi T, Kosaki K	Concurrent deletion of BMP4 and OTX2 genes, two master genes in ophthalmogenesis	Eur J Med Genet.	56(1)	50-53	2013
Takenouchi T, Okuno H, Kosaki R, Ariyasu D, Torii C, Momoshima S, Harada N, Yoshihashi H, Takahashi T, Awazu M, Kosaki K.	Microduplication of Xq24 and Hartsfield syndrome with holoprosencephaly, ectrodactyly, and clefting.	Am J Med Genet A.	158A (10)	2537-2541	2012
Takenouchi T, Enomoto K, Nishida T, Torii C, Okazaki T, Takahashi T, Kosaki K.	12q14 microdeletion syndrome and short stature with or without relative macrocephaly.	Am J Med Genet A	158A (10)	2542-2544	2012
Kosaki R, Kaneko T, Torii C, Kosaki K.	EEC syndrome-like phenotype in a patient with an IRF6 mutation.	Am J Med Genet A	158(5)	1219-1220	2012
Asakura Y, Muroya K, Sato T, Kurosawa K, Nishimura G, Adachi M.	First case of a Japanese girl with Myre syndrome due to a heterozygous SMAD4 mutation.	Am J Med Genet A.	158	Jun-82	2012
Miyazaki O, Nishimura G, Sago H, Horiuchi T, Hayashi S, Kosaki R.	Prenatal diagnosis of fetal skeletal dysplasia with 3D CT.	Pediatr Radiol.	42(7)	842-52	2012

Okamoto N, Hayashi S, Masui A, Kosaki R, Oguri I, Hasegawa T, Imoto I, Makita Y, Hata A, Moriyama K, Inazawa J.	Deletion at chromosome 10p11.23-p12.1 defines characteristic phenotypes with markedmidface retrusion.	J Hum Genet.	57(3)	191-6	2012
Misako Naiki,,Seiji Mizuno,Kenichiro Yamada, Yasukazu Yamada, Reiko Kimura, Makoto Oshiro, Nobuhiko Okamoto, Yoshio Makita, Mariko Seishima, and Nobuaki Wakamatsu	MBTPS2 mutation causes BRESEK/BRESHECK syndrome	Am J Med Genet	158A	97-102	2012
Shimojima K, Okamoto N, Suzuki Y, Saito M, Mori M, Yamagata T, Momoi MY, Hattori H, Okano Y, Hisata K, Okumura A, Yamamoto T.	Subtelomeric deletions of 1q43q44 and severe brain impairment associated with delayed myelination.	J Hum Genet.	57	593-600	2012
Wada Y, Kadoya M, Okamoto N.	Mass spectrometry of apolipoprotein C-III, a simple analytical method for mucin-type O-glycosylation and its application to an autosomal recessive cutis laxa type-2 (ARCL2) patient.	Glycobiology.	22	1140-1144	2012
Hotta K, Nashimoto A, Yasumura E, Suzuki M, Azuma M, Iizumi Y, Shima D, Nabeshima R, Hiramoto M, Okada A, Sakata-Sogawa K, Tokunaga M, Ito T, Ando H, Sakamoto S, Kabe Y, Aizawa S, Imai T, Yamaguchi Y, Watanabe H, Handa H.	Vesnarinone Suppresses TNFα mRNA Expression by Inhibiting Valosin-containing Protein	Mol Pharmacol		In press	2014

〔V〕

研究成果の刊行物・別冊

RESEARCH ARTICLE

AMERICAN JOURNAL OF medical genetics PART A

MBTPS2 Mutation Causes BRESEK/BRESHECK Syndrome

Misako Naiki,[1,2] Seiji Mizuno,[3] Kenichiro Yamada,[1] Yasukazu Yamada,[1] Reiko Kimura,[1] Makoto Oshiro,[4] Nobuhiko Okamoto,[5] Yoshio Makita,[6] Mariko Seishima,[7] and Nobuaki Wakamatsu[1]*

[1]Department of Genetics, Institute for Developmental Research, Aichi Human Service Center, Kasugai, Aichi, Japan

[2]Department of Pediatrics, Nagoya University Graduate School of Medicine, Nagoya, Aichi, Japan

[3]Department of Pediatrics, Central Hospital, Aichi Human Service Center, Kasugai, Aichi, Japan

[4]Department of Pediatrics, Japanese Red Cross Nagoya Daiichi Hospital, Nagoya, Aichi, Japan

[5]Department of Medical Genetics, Osaka Medical Center and Research Institute for Maternal and Child Health, Izumi, Osaka, Japan

[6]Education Center, Asahikawa Medical University, Asahikawa, Hokkaido, Japan

[7]Department of Dermatology, Gifu University Graduate School of Medicine, Gifu, Gifu, Japan

Received 25 July 2011; Accepted 17 October 2011

BRESEK/BRESHECK syndrome is a multiple congenital malformation characterized by brain anomalies, intellectual disability, ectodermal dysplasia, skeletal deformities, ear or eye anomalies, and renal anomalies or small kidneys, with or without Hirschsprung disease and cleft palate or cryptorchidism. This syndrome has only been reported in three male patients. Here, we report on the fourth male patient presenting with brain anomaly, intellectual disability, growth retardation, ectodermal dysplasia, vertebral (skeletal) anomaly, Hirschsprung disease, low-set and large ears, cryptorchidism, and small kidneys. These manifestations fulfill the clinical diagnostic criteria of BRESHECK syndrome. Since all patients with BRESEK/BRESHECK syndrome are male, and X-linked syndrome of ichthyosis follicularis with atrichia and photophobia is sometimes associated with several features of BRESEK/BRESHECK syndrome such as intellectual disability, vertebral and renal anomalies, and Hirschsprung disease, we analyzed the causal gene of ichthyosis follicularis with atrichia and photophobia syndrome, *MBTPS2*, in the present patient and identified an p.Arg429His mutation. This mutation has been reported to cause the most severe type of ichthyosis follicularis with atrichia and photophobia syndrome, including neonatal and infantile death. These results demonstrate that the p.Arg429His mutation in *MBTPS2* causes BRESEK/BRESHECK syndrome.

Key words: BRESEK/BRESHECK syndrome; IFAP syndrome; *MBTPS2*; mutation; S2P

How to Cite this Article:
Naiki M, Mizuno S, Yamada K, Yamada Y, Kimura R, Oshiro M, Okamoto N, Makita Y, Seishima M, Wakamatsu N. 2011. *MBTPS2* mutation causes BRESEK/BRESHECK syndrome.
Am J Med Genet Part A .

INTRODUCTION

BRESEK/BRESHECK syndrome (OMIM# 300404), a multiple congenital malformation disorder characterized by brain anomalies, intellectual disability, ectodermal dysplasia, skeletal deformities, Hirschsprung disease, ear or eye anomalies, cleft palate or cryptorchidism, and kidney dysplasia/hypoplasia [Reish et al., 1997]. The acronym BRESEK refers to the common findings, whereas BRESHECK refers to all manifestations. Because the first two patients were maternally related half brothers, an X-linked disorder was proposed. Although each symptom of these patients is often observed in other congenital diseases, the combination of all symptoms is rare, and only one additional patient with BRESEK has been reported to date [Tumialán and Mapstone, 2006]. Here, we present the fourth male patient with multiple anomalies. The patient presented with a variety of clinical features that were consistent with those of the previously reported BRESHECK syndrome.

The syndrome of ichthyosis follicularis with atrichia and photophobia (IFAP, OMIM# 308205), an X-linked recessive oculocutaneous disorder, is characterized by a peculiar triad of ichthyosis follicularis, total or subtotal atrichia, and varying degrees

Grant sponsor: Takeda Science Foundation; Grant sponsor: Health Labour Sciences Research Grant.
*Correspondence to:
Nobuaki Wakamatsu, Department of Genetics, Institute for Developmental Research, Aichi Human Service Center, 713-8 Kamiya-cho, Kasugai, Aichi 480-0392, Japan. E-mail: nwaka@inst-hsc.jp
Published online 00 Month 2011 in Wiley Online Library (wileyonlinelibrary.com).
DOI 10.1002/ajmg.a.34373

of photophobia [MacLeod, 1909]. Martino et al. [1992] reported a male patient with IFAP syndrome presented with short stature, intellectual disability, seizures, hypohidrosis, enamel dysplasia, congenital aganglionic megacolon, inguinal hernia, vertebral and renal anomalies, and the classic symptom triad of IFAP syndrome. This report broadened the clinical features of IFAP syndrome. It should be noted that the clinical symptoms of this patient are quite similar to those of BRESHECK syndrome, with the exception of cleft palate, cryptorchidism, and photophobia (Patient 5; Table I). The gene mutated in patients with IFAP syndrome, *MBTPS2* (GenBank reference sequence NM_015884), was identified from a variety of clinical features of IFAP syndrome, including the triad and neonatal death [Oeffner et al., 2009]. Thus, the mode of inheritance and several clinical features are common to both BRESEK/BRESHECK and IFAP syndromes. These findings prompted us to perform mutation analysis of *MBTPS2* in the present patient, resulting in the identification of a missense mutation.

MATERIALS AND METHODS

Patients

Written informed consent was obtained from the parents of the patient. Experiments were conducted after approval of the institutional review board of the Institute for Developmental Research, Aichi Human Service Center. The patient (II-1; Fig. 3) was born to a 31-year-old mother (I-2) and a 31-year-old father (I-1), both healthy Japanese individuals without consanguinity. His mother miscarried her first child at 5 weeks. The pregnancy of the patient reported here was complicated with mild oligohydramnios, and he was delivered by caesarean because of a breech position at 38 weeks of gestation. His birth weight was 1,996 g (−2.6 SD), and he measured 44 cm (−2.6 SD) in length with an occipitofrontal circumference of 32.5 cm (−0.5 SD). Apgar scores at 1 and 5 min were four and eight, respectively. The patient exhibited generalized alopecia and lacked eyelashes, scalp hair, and eyebrows (Fig. 1A). The skin on the entire body was erythematous with

TABLE I. Clinical Features of BRESEK/BRESHECK and IFAP Syndromes and *MBTPS2* Mutation

	BRESEK/BRESHECK syndrome				IFAP syndrome		
Patient	**1**	**2**	**3**	**4**	**5**	**6**	**7**
Clinical features							
Gender	M	M	M	M	M	M	M
Gestational age (weeks)	32	40	ND	38	30	ND	ND
Birth weight (g)	990	2,230	ND	1,996	2,040	ND	ND
Intrauterine growth retardation	+	+	ND	+	−	ND	ND
Major features							
Follicular ichthyosis	−	−	ND	−	+	+	+
Atrichia	+	+	+	+	+	+	+
Photophobia	−	−	−	+	+	+	+
Brain malformation	+	+	+	+	+	−	+
Mental and growth retardation	+	+	+	+	+	+	+
Skeletal (Vertebrate) anomalies	+	+	+	+	+	+	+
Hirschsprung disease	−	+	+	+	+	+	+
Eye malformation or	+	+	+	−	+	−	−
Large ears	+	+	+	+	+	−	−
Cleft lip/palate or	−	+	−	−	−	+	−
Cryptorchidism	+	+	−	+	−	−	−
Kidney malformation	+	+	−	+	+	+	+
Other features							
Microcephaly	+	+	+	+	+	−	+
Seizures	−	+	+	+	+	−	+
Deafness	−	+	−	+	−	−	−
Hand anomalies	+	+	+	−	+	+	+
Cardiac anomalies	−	−	+	−	−	−	+
Inguinal hernia	−	−	−	−	+	+	+
Trachea anomalies	−	−	−	+	−	−	−
Regression	−	−	−	+	−	−	−
Age	6 h d	7 y	1.5 y	8 y	3 y	9 m d	14 m d
MBTPS2 mutation	NP	NP	NP	R429H	NP	R429H	R429H

+, present; −, not present; M, male; ND, not described; NP, not performed; h, hour; d, dead; m, month; y, year; R429H, Arg429His; BRESEK/BRESHECK syndrome, [Patients 1-4]; IFAP syndrome, [Patients 5–7]; Patients: 1, Reish et al. [1997] patient 1; 2, Reish et al. [1997] patient 2; 3, Tumialán and Mapstone [2006]; 4, present case; 5, Martino et al. [1992]; 6, Oeffner et al. [2009] 3-III:3; 7, Oeffner et al. [2009] 3-III:4.

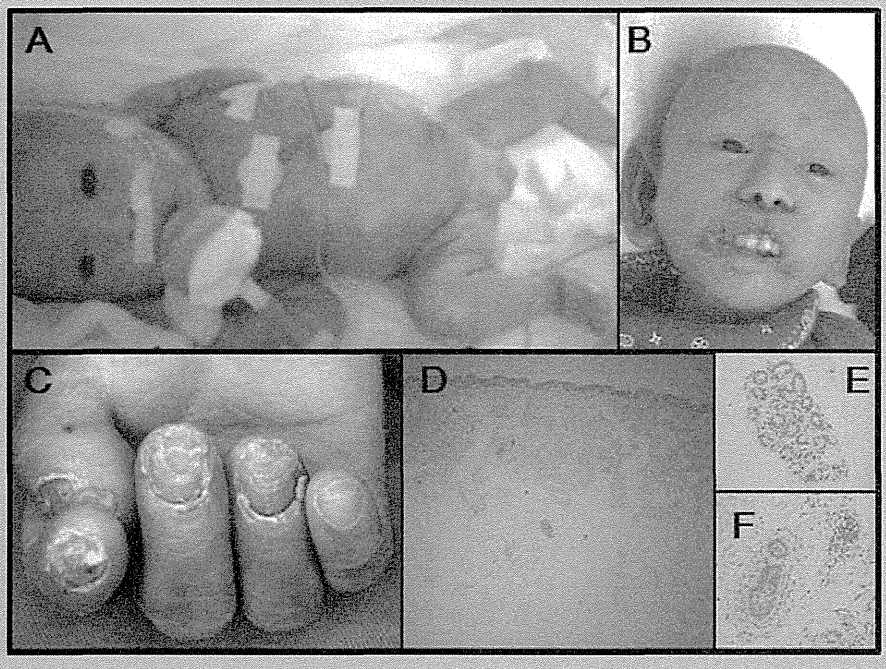

FIG. 1. Clinical appearance and dermatological findings of the patient. A: Lateral view of the patient at birth. Note the generalized alopecia with an absence of scalp hair, eyebrows, and eyelashes. The skin was dry and scaly, and an itchy erythema was observed over the entire body. B: Frontal view of the patient at 4 years of age. Note the characteristic facial appearance with long, malformed ears, a relatively high nasal bridge, and a wide nasal base. C: The patient had normal-sized but deformed and thickened nails. D–F: Histologic examination of the abdominal skin at the age of 15 months showed a reduced number of hair follicles (D), normal eccrine glands (E), and hypoplastic hair follicles (F).

continuous desquamation (Fig. 1A). He had malformed large ears, an inferiorly curved penis, and a bifid scrotum. The testicles were not palpable. He experienced persistent constipation, and total colonic Hirschsprung disease was confirmed through barium enema (Fig. 2E) and rectal biopsy at 2 months. A bone survey performed using three-dimensional (3D) computed tomography (CT) showed abnormal imbalanced hemivertebrae in the two lowest thoracic vertebral bodies (Fig. 2C). The patient's right kidney was smaller than normal. Brain magnetic resonance imaging (MRI) at 3 years of age demonstrated decreased volumes of the frontal and parietal lobes and thinning of the corpus callosum with dilatation of the ventricles (Fig. 2A,B). There were no abnormalities of the eyes or optic nerves. We concluded that the patient had BRESHECK syndrome. The patient had seizures at 5 months of age with an apneic episode and cyanosis. Electroencephalographic (EEG) analysis showed abnormal patterns of sharp waves in the posterior lobe. The seizures were almost completely controlled with phenobarbital. The patient was allergic to milk. At 7 months, tracheal endoscopy revealed subglottic tracheal stenosis and abnormal segmentation of the left lung. A chest CT performed at 3 years of age showed a congenital cystic adenomatoid malformation (CCAM) in the right upper lobe (Fig. 2D). Auditory brain stem responses showed bilateral 80 dB hearing loss at 8 months of age.

The patient exhibited delayed psychomotor development during his infancy. He could drink from a bottle at the age of 3 months and could sit up unsupported at 15 months. Abdominal skin biopsy at 15 months revealed reduced number of hair follicles (Fig. 1D). The eccrine glands were normal (Fig. 1E), and most of his hair follicles appeared to be hypoplastic (Fig. 1F). These findings were similar to ichthyosiform erythroderma. Photophobia was noted when the patient left the hospital and first went outside at 18 months of age. At 2 years and 6 months of age, he had a series of epileptic episodes. He experienced a maximum of 100 seizures per day, and EEG analysis showed continual abnormal spikes in the posterior lobe. The seizures were controlled with clonazepam therapy. At 2 years and 9 months of age, he could stand with support and displayed social smiles when interacting with other people. However, the patient developed psychomotor regression at the age of 3 years. He exhibited a progressive loss of emotional response to others, developed hypotonia, and could not stand or sit alone. At 4 years of age, he became bedridden and showed almost no response to people. He had highly desquamated skin, similar to that seen in ichthyosis (Fig. 1B), and easily developed erythema on the skin of the entire body. The patient had deformed and thickened nails (Fig. 1C). He had persistent corneal erosions, but ophthalmoscopy could not be performed at the age of 4 years because of corneal opacification.

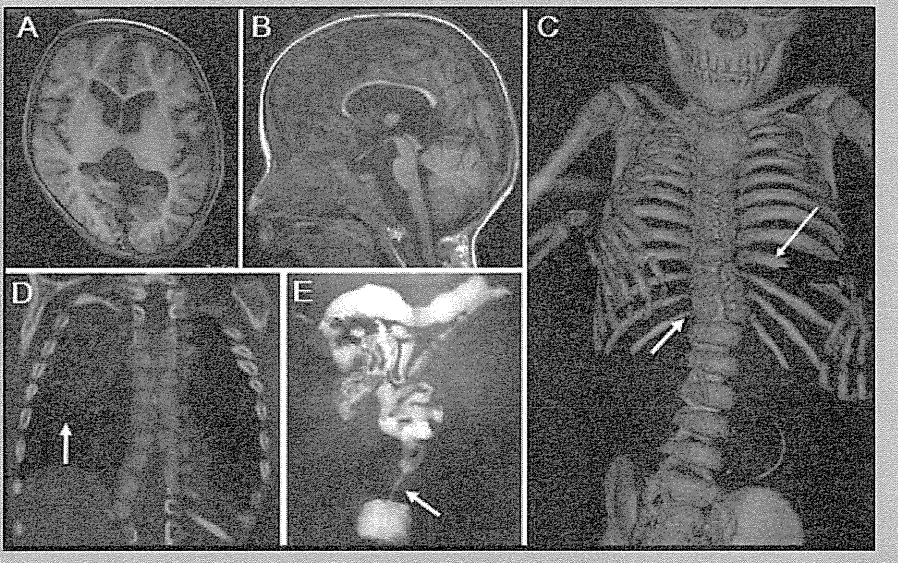

FIG. 2. CT and MRI findings of the patient. A,B: Brain MRI (T1-weighted image) at 3 years of age showed decreased volume of the cortex in the frontal and parietal lobes, the presence of a subdural cyst in the corpora quadrigemina, and dilatation of the lateral and fourth ventricle. C: A bone survey performed using 3D CT showed abnormal segmentation of the ninth rib and an imbalanced hemivertebrae in the two lowest thoracic vertebral bodies (shown with arrows). D: CT of the chest showed CCAM (indicated by the arrow) in the right upper lobe. E: Barium enema showed a reduced caliber rectum (indicated by the arrow), suggesting that the patient had Hirschsprung disease.

Chromosomal and Molecular Genetic Studies

Genomic DNA isolated from the patient's peripheral white cells by phenol/chloroform extraction was used for *MBTPS2* mutation analysis. PCR-amplified DNA fragments were isolated using the QIAEX II Gel Extraction Kit (Qiagen, Valencia, CA) and purified using polyethylene glycol 6000 precipitation. PCR products were sequenced with the Big Dye Terminator Cycle Sequencing Kit V1.1 and analyzed with the ABI PRISM 310 Genetic Analyzer (Life Technologies, Carlsbad, CA). We also performed G-banded chromosome analysis at a resolution of 400–550 bands, genome-wide subtelomere fluorescence in situ hybridization (FISH) analysis, and array comparative genomic hybridization (array CGH) using Whole Human Genome Oligo Microarray Kits 244K (Agilent Technologies Inc., Palo Alto, CA) to identify genomic abnormalities.

RESULTS

G-banded chromosome analysis and genome-wide subtelomere FISH analyses did not show chromosomal rearrangements in the patient. Array CGH analysis did not show copy number changes in the patient's genome with the exception of known copy-number variations (CNVs). Since some patients with IFAP syndrome have been reported to present with several clinical features of BRESEK/BRESHECK syndrome, including severe intellectual disability, vertebral and renal anomalies, and Hirschsprung disease, we conducted a comprehensive sequencing analysis of all exons and intron–exon boundaries of *MBTPS2*. This analysis identified a missense mutation (c.1286G>A, [p.Arg429His]) in exon 10, which was previously reported for IFAP syndrome (Fig. 3). The mutation was also found in one allele of the mother (I-2), indicating that the mutation was of maternal origin and that the mother was a heterozygous carrier (Fig. 3).

DISCUSSION

In this report, we describe the fourth male patient with BRESHECK syndrome in whom we identified a missense mutation (c.1286G>A, [p.Arg429His]) in *MBTPS2*, which is the causal gene for IFAP syndrome. *MBTPS2* encodes a membrane-embedded zinc metalloprotease, termed site-2 protease (S2P). S2P cleaves and activates cytosolic fragments of sterol regulatory element binding proteins (SREBP1 and SREBP2) and a family of bZIP membrane-bound transcription factors of endoplasmic reticulum (ER) stress sensors (ATF6, OASIS), after a first luminal proteolytic cut by site-1 protease (S1P) within Golgi membranes [Sakai et al., 1996; Ye et al., 2000; Kondo et al., 2005; Asada et al., 2011]. The SREBPs control the expression of many genes involved in the biosynthesis and uptake of cholesterol, whereas ATF6 and OASIS induce many genes that clean up accumulated unfolded proteins in the ER. Dysregulated SREBP activation, impaired lipid metabolism, and accumulation of unfolded proteins in the ER caused by *MBTPS2* mutations could lead to disturbed differentiation of epidermal structures, resulting in the symptom triad of IFAP syndrome [Cursiefen et al., 1999; Traboulsi et al., 2004; Elias et al., 2008]. Oeffner et al. [2009] first identified five missense mutations in *MBTPS2* in patients with IFAP

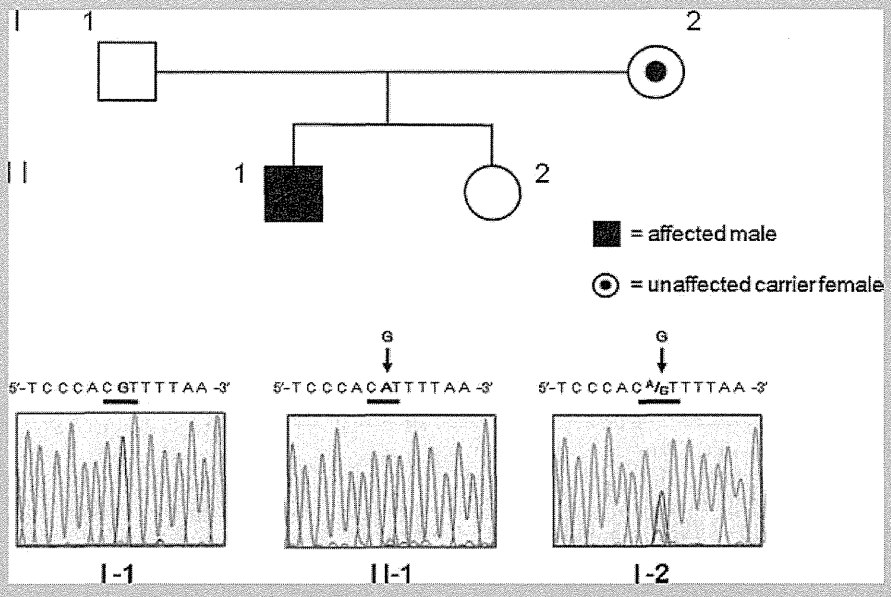

FIG. 3. Identification of a disease mutation. The sequence analyses of the patient (II-1) showed a c.1286G>A variant in exon 10 of *MBTPS2*, which predicts p.Arg429His, as indicated by the arrow (middle panel). The mother (I-2) was heterozygous for the mutation ($C^A/_GT$) (right panel).

syndrome. Transfection studies using wild type and mutant *MBTPS2* expression constructs demonstrated that the five *MBTPS2* mutations did not affect S2P protein amount and localization in the ER. However, enzyme activities, as measured by sterol responsiveness, were decreased in S2P-deficient M19 cells when the mutant *MBTPS2* was transiently expressed. Interfamilial phenotypic differences between male IFAP patients and the properties of mutants in functional assays predict a genotype–phenotype correlation, ranging from mild forms of the triad with relatively high enzyme activity (~80%) to severe manifestations of intellectual disability, various developmental defects, and early death with low enzyme activity (~15%). The identified p.Arg429His mutation in the patient reported here is one of the five missense mutations with the lowest enzyme activity. It was previously reported that all four patients harboring the p.Arg429His mutation died within 14 months of birth. The five mutations were not located in the HEIGH motif (amino acids [aa] 171–175) or in the $LD_{467}G$ sequence, both of which are regions important for coordinating the zinc atom at the enzymatic active site for protease activity in the Golgi membrane [Zelenski et al., 1999]. However, among the five mutations, the p.Arg429His mutation is located closest to the intramembranous domain, and it strongly reduced the enzymatic activity and caused a severe phenotype. This finding suggests that mutations in the HEIGH motif or in the $LD_{467}G$ sequence are fatal because they lead to a null function of the S2P. Although the detailed skin findings of the four patients with the p.Arg429His mutation have not been reported, it should be noted that one of the four patients (3-III:4) with the p.Arg429His mutation had brain anomaly, seizures, psychomotor retardation, vertebrae anomaly, Hirschsprung disease, absence of a kidney, atrial septum defect, and inguinal hernia, in addition to the symptom triad of IFAP syndrome [Oeffner et al., 2009]. These symptoms overlap with the majority of symptoms observed in BRESHECK syndrome (BRESHK; six of eight symptoms observed in BRESHECK) (Table I), and the present patient has BRESHECK syndrome. Collectively, these observations suggest that the most severe form of the syndrome caused by the p.Arg429His mutation in *MBTPS2* shows features quite similar or identical to those of BRESEK/BRESHECK syndrome.

There are two major differences in the definitions of IFAP syndrome and BRESEK/BRESHECK syndrome. Ichthyosis follicularis, one of the triad symptoms of IFAP syndrome, is a clinical condition of the skin. However, several studies on IFAP syndrome have reported various skin eruptions such as psoriasis-like and ichthyosis-like eruptions [Martino et al., 1992; Sato-Matsumura et al., 2000]. In contrast, patients with BRESEK/BRESHECK syndrome showed severe lamellar desquamation with diffuse scaling [Reish et al., 1997], similar to that observed in the present patient. This could be because of the difference in features of the skin, namely, ichthyosiform erythroderma-like appearance versus ichthyosis follicularis, in patients with the most severe forms of *MBTPS2* mutation and patients with IFAP syndrome who were described earlier, respectively.

The second difference is that photophobia was not described in the reported three male patients with BRESEK/BRESHECK syndrome [Reish et al., 1997; Tumialán and Mapstone, 2006]. In the present patient, photophobia became evident after he was diagnosed with BRESHECK syndrome. Photophobia is a symptom of epithelial disturbances of the cornea, such as ulceration and vascularization, which result in corneal scarring [Traboulsi et al., 2004]. In the most severe cases of *MBTPS2* mutation, such as

patients with severe intellectual disability who are bedridden and die early, it is likely that the patients were treated in the hospital without being exposed to sunlight. Therefore, it would be difficult to observe photophobia as a main symptom in those cases. Moreover, two previously described patients with BRESEK/BRESHECK syndrome had initial maldevelopment of one eye or small optic nerves. In these patients, photophobia may not have been obvious because of malformations of the eyes and optic nerves [Reish et al., 1997]. In our study, the patient showed clinical features of BRESHECK syndrome and photophobia with *MBTPS2* mutation, indicating that the clinical features of the present patient are extremely broad compared to the features of IFAP syndrome caused by *MBTPS2* mutation that have been previously reported [MacLeod, 1909].

Recently, a missense mutation (c.1523A>G, [p.Asn508Ser]) in *MBTPS2* was identified from 26 cases of three independent families with keratosis follicularis spinulosa decalvans (KFSD; OMIM# 308800), which is characterized by the development of hyperkeratotic follicular papules on the scalp followed by progressive alopecia of the scalp, eyelashes, and eyebrows in addition to childhood photophobia and corneal dystrophy [Aten et al., 2010]. A significant association was found between KFSD and the p.Asn508Ser mutation. The specific localization of alopecia to the scalp, eyelashes, and eyebrows and the limited childhood photophobia of KFSD indicate that KFSD has a relatively mild phenotype. The authors postulate that IFAP syndrome and KFSD are within the spectrum of one genetic disorder with a partially overlapping phenotype and propose that a new name should be chosen for KFSD/IFAP syndrome with an *MBTPS2* mutation. In contrast, the BRESHECK syndrome observed in the present patient has a severe phenotype caused by the p.Arg429His mutation. The present patient and the two patients (3-III:3 and 3-III:4) with the p.Arg429His mutation displayed broader clinical features, including eight features (BRESHECK) and six features (RESHCK and BRESHK) of BRESEK/BRESHECK syndrome, respectively (patients 4, 6, and 7; Table I) [Oeffner et al., 2009]. There is a debate regarding whether the two patients harboring six features were correctly diagnosed with BRESEK/BRESHECK syndrome since the patients did not have "BRESEK" but rather a combination of six other clinical features. To better understand and clearly distinguish the clinical features of the present patient from those of the reported patients with *MBTPS2* mutations, we propose the nomenclature of "BRESHECK/IFAP syndrome" for the present patient because he has clinical features of BRESHECK syndrome. We also suggest that the BRESHECK/IFAP syndrome be used for a broader definition that would include patients harboring most features of BRESHECK syndrome, including the previously reported two patients (3-III:3 and 3-III:4) with p.Arg429His mutation in *MBTPS2* [Oeffner et al., 2009]. Data from further genetic and clinical studies on more patients are required to determine which genes or *MBTPS2* mutations are associated with BRESEK/BRESHECK or BRESHECK/IFAP syndrome, respectively.

ACKNOWLEDGMENTS

We thank the patient and his family for participating in the study. This study was supported by the Takeda Science Foundation (to N.W.) and by the Health Labour Sciences Research Grant (to S.M. and N.W.).

REFERENCES

Aten E, Brasz LC, Bornholdt D, Hooijkaas IB, Porteous ME, Sybert VP, Vermeer MH, Vossen RH, van der Wielen MJ, Bakker E, Breuning MH, Grzeschik KH, Oosterwijk JC, den Dunnen JT. 2010. Keratosis follicularis spinulosa decalvans is caused by mutations in MBTPS2. Hum Mutat 31:1125–1133.

Asada R, Kanemoto S, Kondo S, Saito A, Imaizumi K. 2011. The signalling from endoplasmic reticulum-resident bZIP transcription factors involved in diverse cellular physiology. J Biochem 149:507–518.

Cursiefen C, Schlötzer-Schrehardt U, Holbach LM, Pfeiffer RA, Naumann GOH. 1999. Ocular findings in ichthyosis follicularis, atrichia, and photophobia syndrome. Arch Ophthalmol 117:681–684.

Elias PM, Williams ML, Holleran WM, Jiang YJ, Schmuth M. 2008. Pathogenesis of permeability barrier abnormalities in the ichthyoses: Inherited disorders of lipid metabolism. J Lipid Res 49:697–714.

Kondo S, Murakami T, Tatsumi K, Ogata M, Kanemoto S, Otori K, Iseki K, Wanaka A, Imaizumi K. 2005. OASIS, a CREB/ATF-family member, modulates UPR signalling in astrocytes. Nat Cell Biol 7:186–194.

MacLeod JMH. 1909. Three cases of 'ichthyosis follicularis' associated with baldness. Br J Dermatol 21:165–189.

Martino F, D'Eufemia P, Pergola MS, Finocchiaro R, Celli M, Giampà G, Frontali M, Giardini O. 1992. Child with manifestations of dermotrichic syndrome and ichthyosis follicularis alopecia photophobia (IFAP) syndrome. Am J Med Genet 44:233–236.

Oeffner F, Fischer G, Happle R, König A, Betz RC, Bornholdt D, Neidel U, Boente Mdel C, Redler S, Romero-Gomez J, Salhi A, Vera-Casaño A, Weirich C, Grzeschik KH. 2009. IFAP syndrome is caused by deficiency in MBTPS2, an intramembrane zinc metalloprotease essential for cholesterol homeostasis and ER stress response. Am J Hum Genet 84:459–467.

Reish O, Gorlin RJ, Hordinsky M, Rest EB, Burke B, Berry SA. 1997. Brain anomalies, retardation of mentality and growth, ectodermal dysplasia, skeletal malformations, Hirschsprung disease, ear deformity and deafness, eye hypoplasia, cleft palate, cryptorchidism, and kidney dysplasia/hypoplasia (BRESEK/BRESHECK): New X-linked syndrome? Am J Med Genet 68:386–390.

Sakai J, Duncan EA, Rawson RB, Hua X, Brown MS, Goldstein JL. 1996. Sterol-regulated release of SREBP-2 from cell membranes requires two sequential cleavages, one within a transmembrane segment. Cell 85: 1037–1046.

Sato-Matsumura KC, Matsumura T, Kumakiri M, Hosokawa K, Nakamura H, Kobayashi H, Ohkawara A. 2000. Ichthyosis follicularis with alopecia and photophobia in a mother and daughter. Br J Dermatol 142:157–162.

Traboulsi E, Waked N, Mégarbané H, Mégarbané A. 2004. Ocular findings in ichthyosis follicularis–alopecia–photophobia (IFAP) syndrome. Ophthal Genet 25:153–156.

Tumialán LM, Mapstone TB. 2006. A rare cause of benign ventriculomegaly with associated syringomyelia: BRESEK/BRESHECK syndrome. Case illustration. J Neurosurg 105:155.

Ye J, Rawson RB, Komuro R, Chen X, Davé UP, Prywes R, Brown MS, Goldstein JL. 2000. ER stress induces cleavage of membrane-bound ATF6 by the same proteases that process SREBPs. Mol Cell 6:1355–1364.

Zelenski NG, Rawson RB, Brown MS, Goldstein JL. 1999. Membrane topology of S2P, a protein required for intramembranous cleavage of sterol regulatory element-binding proteins. J Biol Chem 274:21973–21980.

Development, Growth & Differentiation
The Japanese Society of Developmental Biologists

Develop. Growth Differ. (2012) **54**, 588–604 doi: 10.1111/j.1440-169X.2012.01362.x

Original Article

Establishment and characterization of Roberts syndrome and SC phocomelia model medaka (*Oryzias latipes*)

Akihiro Morita,[1,*,†] Kumiko Nakahira,[1] Taeko Hasegawa,[1] Kaoru Uchida,[1] Yoshihito Taniguchi,[2,‡] Shunichi Takeda,[2] Atsushi Toyoda,[3,§] Yoshiyuki Sakaki,[3,¶] Atsuko Shimada,[4] Hiroyuki Takeda[4] and Itaru Yanagihara[1,*]

[1]*Department of Developmental Medicine, Research Institute, Osaka Medical Center for Maternal and Child Health, Izumi, Osaka,* [2]*Department of Radiation Genetics, Faculty of Medicine, Kyoto University, CREST, Japan Science and Technology Laboratory, Kyoto,* [3]*Sequence Technology Team, RIKEN Genomic Sciences Center, Yokohama, Kanagawa, and* [4]*Department of Biological Sciences, Graduate School of Science, University of Tokyo, Tokyo, Japan*

Roberts syndrome and SC phocomelia (RBS/SC) are genetic autosomal recessive syndromes caused by *establishment of cohesion 1 homolog 2* (*ESCO2*) mutation. RBS/SC appear to have a variety of clinical features, even with the same mutation of the *ESCO2* gene. Here, we established and genetically characterized a medaka model of RBS/SC by reverse genetics. The RBS/SC model was screened from a mutant medaka library produced by the Targeting Induced Local Lesions in Genomes method. The medaka mutant carrying the homozygous mutation at R80S in the conserved region of ESCO2 exhibited clinical variety (i.e. developmental arrest with craniofacial and chromosomal abnormalities and embryonic lethality) as characterized in RBS/SC. Moreover, widespread apoptosis and downregulation of some gene expression, including *notch1a*, were detected in the R80S mutant. The R80S mutant is the animal model for RBS/SC and a valuable resource that provides the opportunity to extend knowledge of ESCO2. Downregulation of some gene expression in the R80S mutant is an important clue explaining non-correlation between genotype and phenotype in RBS/SC.

Key words: *ESCO2*, *Oryzias latipes*, premature chromosomal separation, Roberts syndrome and SC phocomelia.

Introduction

Roberts syndrome (RBS) (Online Mendelian Inheritance in Man [OMIM] 268300) is a genetic autosomal recessive syndrome. RBS is characterized by intrauterine fetal death, failure to thrive, mental and growth retardation, microcephaly, cleft lip and palate, and symmetrical limb defects (Vega *et al.* 2010). Chromosomal abnormality, for example, premature centromere separation (PCS), in the metaphase RBS cell is also observed. Recently, we identified *establishment of cohesion 1 homolog 2* (*ESCO2*) as the gene responsible for RBS (Vega *et al.* 2005). Similar pathological features, although milder than RBS, are observed in SC phocomelia (SC) (OMIM 269000). SC is also an autosomal recessive disorder caused by *ESCO2* mutation (Schüle *et al.* 2005). In spite of the mutation being in the same gene, different diagnoses were previously made. Both RBS and SC were caused by truncating mutations (either nonsense mutation or frame-shift), eliminating the functionally important acetyltransferase domain, except for one family in which RBS was caused by the missense mutation in the acetyltransferase domain (Schüle *et al.* 2005; Vega *et al.* 2005, 2010; Gordillo *et al.* 2008). Gordillo *et al.* (2008) considered that RBS and SC were the same syndrome with varying phenotypic expression. Thus, clinical

*Authors to whom all correspondence should be addressed.
Email: morita-a@suzuka-u.ac.jp; itaruy@mch.pref.osaka.jp
†Present address: Faculty of Pharmaceutical Sciences, Suzuka University of Medical Science, Suzuka, Mie 513-8670, Japan.
‡Present address: Department of Preventive Medicine and Public Health, School of Medicine, Keio University, Shinjuku-ku, Tokyo 160-8582, Japan.
§Present address: Comparative Genomics Laboratory, Center for Genetic Resource Information, National Institute of Genetics, Mishima, Shizuoka 411-8540, Japan.
¶Present address: Toyohashi University of Technology, Toyohashi, Aichi 441-8580, Japan.
Received 28 September 2011; revised 25 April 2012; accepted 9 May 2012.

features are considerably different in severity, suggesting there is no phenotype–genotype correlation.

The expression of *ESCO2* is dependent on the cell cycle, namely, it is expressed in the S-phase (Whitfield *et al.* 2000; Nishihara *et al.* 2010). *ESCO2* is a homologue of *Ctf7/Eco1* in the yeast *Saccharomyces cerevisiae* (Hou & Zou 2005). *ESCO2* and *Eco1* encode a member of the acetyltransferase family (Skibbens *et al.* 1999; Vega *et al.* 2010). The ECO1 protein lacks the N-terminal half of ESCO2. ECO1 and the C-terminal half of ESCO2 contain a PIP box, a C2H2 zinc finger and an acetyltransferase domain. PIP box and C2H2 zinc finger domains are involved in the interaction with proliferating cell nuclear antigen (Moldovan *et al.* 2006) and acetylation of cohesin subunits (Ivanov *et al.* 2001; Hou & Zou 2005; Rolef Ben-Shahar *et al.* 2008; Unal *et al.* 2008; Zhang *et al.* 2008; Onn *et al.* 2009), respectively. Cohesin acetylation by ESCO2 and ECO1 is a central determinant of replication fork processivity (Terret *et al.* 2009) and is essential for the establishment of cohesion from yeast to humans (Skibbens *et al.* 1999; Hou & Zou 2005).

Medaka (*Oryzias latipes*) and zebrafish (*Danio rerio*) are attractive vertebrate animal models because of their easy handling and large numbers of progeny per generation. To analyze gene function, an easy knockdown method using a morpholino injection has been established. Furthermore, medaka is suitable for genetic analysis because it has a lower ploidy level than zebrafish (Ishikawa 2000), and a high quality draft genome sequence of medaka (Kasahara *et al.* 2007) and large numbers of mutants (Furutani-Seiki *et al.* 2004) are available. In this study, we employed a reverse genetic approach in mutant medaka (*O. latipes*) produced using the Targeting Induced Local Lesions in Genomes (TILLING) method (Taniguchi *et al.* 2006) for translational research to explain RBS/SC pathobiology through the *ESCO2* mutation. The expression pattern of *ESCO2* in medaka is similar to that in humans. *ESCO2* mutant medaka showed RBS/SC-like divergence in their phenotype. This *ESCO2* mutant medaka is the animal model for RBS/SC. Moreover, downregulation of *notch1a* and its downstream gene expression was observed in *ESCO2* mutants. This is an important clue explaining the clinical variety of RBS/SC.

Materials and methods

Fish strain and embryos

This study was performed using K-Cab, a substrain of Cab, and K-Kaga, a northern strain of medaka. K-Kaga was a kind gift from the National BioResource Project Medaka. The mutant strains were derived from K-Cab (Taniguchi *et al.* 2006). Eggs were collected from a laboratory colony. Embryos were incubated at 28.5°C after collection, and were staged according to Iwamatsu (1994).

Cloning of medaka ESCO2

A partial cDNA sequence of medaka *ESCO2* was obtained from a genome database (University of Tokyo Genome Browser Medaka [http://utgenome.org/medaka/]), and was amplified using the primers (*ESCO2* cloning primers, see Table S1). Because the 5′ part was missing from the database, rapid amplification of 5′ cDNA ends (5′-RACE) was performed using the SMART RACE cDNA Amplification Kit (Clontech). Two rounds of 5′-RACE were performed with cDNA prepared from embryos using the gene-specific primers (*ESCO2* RACE primers, see Table S1). The cDNA fragment of *ESCO2* (5′-untranslated region and open reading frame [ORF]) was amplified by polymerase chain reaction (PCR) from embryonic cDNA library using *ESCO2* full forward and reverse as primers, and was cloned into pSTBlue-1 vector (Novagen).

In situ *hybridization*

cDNA sequences of medaka *β-actin*, *lfng* and *myf5* were obtained from a genome database (Ensembl genome browser in medaka [http://uswest.ensembl.org/Oryzias_latipes/Info/Index]; accession no., *β-actin*, ENSORLT00000017152; *lfng*, ENSORLT00000005779; *myf5*, ENSORLT00000020353). cDNA fragments were cloned into pSTBlue-1 (Novagen) vector by reverse transcription (RT)–PCR using each primer set (see Table S1) and sequenced for confirmation. The other genes were previously cloned into vectors (Kage *et al.* 2004). The RNA probes were produced by *in vitro* transcription by using SP6, T7 or T3 RNA polymerase (Roche Applied Science) and DIG RNA Labeling Mix (Roche Applied Science) according to the manufacturer's instruction. Whole-mount *in situ* hybridization was performed as previously described (Terasaki *et al.* 2006). The fixative solution was modified as follows: 4% paraformaldehyde (PFA) in 0.85× phosphate-buffered saline containing Tween-20 (0.1%, 0.85× PBST) and 1.5× PBST, which were used for the embryos at the gastrula stage (stage 16) and at other stages, respectively. The length of proteinase K treatment was modified as follows: 0, 1, 7 and 12 min for the embryos at stage 11 or earlier, 12–18, 19–24 and 25 or later, respectively. The samples were observed using a microscope (Olympus BX51).

Cartilage staining

Cartilage staining was performed according to Yasutake *et al.* (2004). The whole-mount and pectoral fin samples were observed by using a stereoscopic microscope (Olympus SZX10) and a microscope (Olympus BX51), respectively.

Immunohistochemistry

Immunohistochemical analysis was performed according to Iijima and Yokoyama (2007) by using anti-phosphorylated histone H3 antibody (Upstate, at 1/100 dilution) and Alexa Fluor 488 anti-rabbit immunoglobulin (Ig)G antibody (Invitrogen, at 1/1000 dilution). The samples were observed by using a fluorescence microscope (Olympus IX71).

5-Bromodeoxyuridine (BrdU) incorporation

Because medaka chorion is almost impermeable to BrdU (Nguyen *et al.* 1999), we injected 0.1% BrdU (in the kit FITC BrdU Flow Kit, BD Biosciences)/Yamamoto solution into the perivitelline space at 2.0 days postfertilization (dpf). Two hours after injection, the embryos were fixed by 4% PFA/PBST. After fixation, the experimental procedure was the same as in immunohistochemistry, but using anti-BrdU antibody (Thermo Scientific, at 1/500 dilution) and Alexa Fluor 488 anti-mouse IgG antibody (Invitrogen, at 1/1000 dilution).

Terminal deoxynucleotidyl transferase-mediated dUTP nick end labeling (TUNEL) assay

A whole-mount TUNEL assay was performed by using an *in situ* Apoptosis Detection Kit (Takara) according to the method of Iijima and Yokoyama (2007) and the manufacturer's instructions. The method was slightly modified as follows: The anti-fluorescein isothiocyanate (anti-FITC) antibody conjugated with horseradish peroxidase in the kit was replaced by anti-FITC antibody conjugated with alkaline phosphatase (at 1/500 dilution), 4-nitro blue tetrazolium chloride (NBT) and 5-bromo-4-chloro-3-indolyl-phosphate, 4-toluidine salt (BCIP) (Roche Applied Science) were used for visualization of apoptotic cells. The samples were observed by using a microscope (Olympus BX51).

Genotyping

Genomic DNA was extracted from whole embryos and caudal fin of fry by treatment of proteinase K (100 μg/mL proteinase K, 10 mmol/L Tris-HCl (pH 8.0), 5 mmol/L ethylenediaminetetraacetic acid, 1% sodium dodecylsulfate), phenol extraction, phenol-chloroform isoamyl alcohol extraction and isopropyl alcohol precipitation. The genomic DNA was subjected to PCR by using a primer set (*ESCO2* Seq1 and *ESCO2* Seq2, see Table S1). After confirmation of amplicon length by separation electrophoresis in agarose gel, PCR products was subjected to direct sequence by using BigDye Terminator (Applied Biosystems), and primers *ESCO2* Seq3 or *ESCO2* Seq2 (see Table S1).

Investigation of the expression allele of ESCO2

First we crossed *ESCO2*$^{240T,\ 242A,\ 581C/240G,\ 242T,\ 581C}$ females and *ESCO2*$^{240G,\ 242A,\ 581A/240G,\ 242A,\ 581A}$ males. At several developmental stages, total RNA extraction by ISOGEN (Nippon Gene) and DNase (in the kit of SV Total RNA Isolation System, Promega) treatment and first strand cDNA production (PrimeScript 1st strand cDNA Synthesis Kit, Takara) was carried out according to the manufacturer's instructions. The first strand cDNA was subjected to PCR using TaKaRa Ex Taq (Takara) and the primer set (*ESCO2* full, see Table S1). The PCR products were separated by agarose electrophoresis. Direct sequencing was performed using the primer *ESCO2* Seq4 or *ESCO2* Seq3 (see Table S1). From the sequence, we assessed the expression alleles as follows: when the nucleotide sequence is 240T/G, 242A/T and 581C, the RNA is derived from two maternal alleles; when it is 240T/G, 242A/T and 581C/A, the RNA is from two maternal and paternal alleles; and when it is 240T/G, 242A and 581C/A or 240G, 242T/A and 581A/C, the RNA is from one maternal and paternal (i.e. embryonic alleles).

Morpholino injection

We constructed three morpholinos as follows: ATG mo, CGGATCATCTTCAGAGTTCACCGTC (start codon underlined); 5mis mo, CGCATGATCTTCACAGTTGACCCTC (mispaired bases underlined); and E2I2 mo, GCTTCCAGGAACCTCCGTACCTGTC (targets 3′-donor of exon 2). Morpholinos (50–300 nmol/L) diluted with Yamamoto solution were injected into one blastomere of one-cell stage embryos (stage 2) using FemtoJet (Eppendorff) and Injectman M2 (Eppendorff) according to the method of Rembold *et al.* (2006) under a stereoscopic microscope (Olympus SZX7).

Chromosomal analysis

Chromosomal analysis was performed according to the method of Westerfield (2000). Briefly, colchicine-treated (400 μg/mL at 28.5°C for 180 min) embryos

were treated with 1.1% trisodium citrate for 16 min. During trisodium citrate treatment, embryos were dechorionated and the yolk was dissected away. After hypotonization (50 mmol/L KCl at 30°C for 15 min), the dissociated cells were fixed using cold Carnoy's fixative for 20 min and washed. The fixed cell solution was divided into two aliquots. One of them was subjected to DNA extraction and genotyping (see genotyping). The other was spotted onto a cold slide glass and re-fixed by flame. The samples were stained using Giemsa solution (4% Giemsa Stock in 10 mmol/L phosphate buffer for 60 min, pH 7) and observed using a microscope (Olympus BX51).

Flow cytometry

Sample preparation was as previously described (Candal *et al.* 2007), but slightly modified. Briefly, after filtration of nuclei from frozen and dechorionized embryos, filtrates were treated with RNase A (100 μg/mL; Wako) and stained with 1 mg/mL propidium iodide (Dojindo). Nuclei (10 000) were analyzed using FACScan (BD Biosciences).

Quantitative RT-PCR

cDNA sequences of *notch1a*, *notch1b*, *notch3*, *ascl1a*, *ascl1b*, *GATA-1* and *EF-1α* were obtained from a genome database (Ensembl genome browser in medaka [http://uswest.ensembl.org/Oryzias_latipes/Info/Index]; accession no.: *notch1a*, ENSORLT00000006535; *notch1b*, ENSORLT00000000793; *notch3*, ENSORLT00000007526; *ascl1a*, ENSORLT00000020662; *ascl1b*, ENSORLT00000015163; *GATA-1*, ENSORLT00000017528; and *EF-1α*, ENSORLT00000009544). cDNA sequences of *sox9b*, *col2a1a* and *col2a1b* were obtained from GenBank (accession no.: *sox9b*, AY870393; *col2a1a*, AB617801; *col2a1b*, AB617803). Total RNA extraction and first strand cDNA production were carried out as described above. Before RT–PCR analysis, we performed sequence analysis of *ESCO2* similar to that performed during the investigation of expression alleles. For quantification of mRNA of *notch1a*, *notch1b*, *notch3*, *ascl1a*, *ascl1b*, *GATA-1* and *EF-1α*, real-time PCR analysis was applied to the first strand cDNA and the plasmid vector containing the target gene (as standard) using Applied Biosystems 7500 Fast RT–PCR System (Applied Biosystems), QuantiTect SYBR Green PCR Kit (Qiagen) and primer sets (see Table S1). For quantification of mRNA of the *sox9b*, *col2a1a* and *col2a1b*, Custum TaqMan Gene Expression Assays (assay name and ID: MFSOX9B, AIGJP3B; MFCOL2A1A, AIHSN9J; MFCOL2A1B, AII1MFR; Applied Biosystems) was used. After estimating the amount of mRNA from the cycle threshold (Ct) value of samples and the standard curve, the amount of mRNA was normalized by the amount of *EF-1α* mRNA and represented by relative abundance against wild-type (WT) embryos. Some amplified fragments were cloned into pT7Blue vector (Novagen) and were sequenced for confirmation.

Statistical analysis

Several statistical analyses were performed according to Zar (2010).

Results

Cloning of medaka ESCO2 *cDNA*

We cloned medaka *ESCO2* cDNA (DNA Data Bank of Japan accession no. AB601774) from embryos. It had a 1590-bp ORF encoding a 530-residue polypeptide, and a 5′-non-coding region of 177 nucleotides. The predicted ESCO2 had a calculated molecular weight of 58.7 kDa. The similarity searches showed that the medaka ESCO2 protein was similar to ESCO2 from several species including humans (Fig. S1). The identities of the medaka ESCO2 protein to that of humans, mice and zebrafish were 52.6%, 55.8% and 47.8%, respectively. Medaka ESCO2 had several conserved regions that consisted of a nuclear localization signal, PIP domain, C2H2-zinc finger domain, acetyltransferase domain and regions with unknown functions.

Expression pattern of ESCO2 *in medaka*

We investigated the *ESCO2* expression pattern during embryogenesis using whole-mount *in situ* hybridization. *ESCO2* mRNA was detected in all blastomeres at stage 5 (Fig. S2) and in the embryonic shield during gastrulation (stage 15–16, Fig. 1A). During early somitogenesis stages, *ESCO2* was expressed throughout the embryonic body, particularly in the optic vesicles, neural tube and somites (Fig. 1B). *ESCO2* expression was limited to the posterior region of optic tectum, prospective corpus cerebelli and pectoral fin buds in late somitogenesis stages at and after stage 28 (Fig. 1C), and to the genital ridge at stage 31 (Fig. 1D). These results are similar to the *ESCO2* expression pattern in human embryos (Vega *et al.* 2010). Because these *ESCO2*-expressing regions are thought to be proliferative zones (Nguyen *et al.* 1999; Candal *et al.* 2007), we

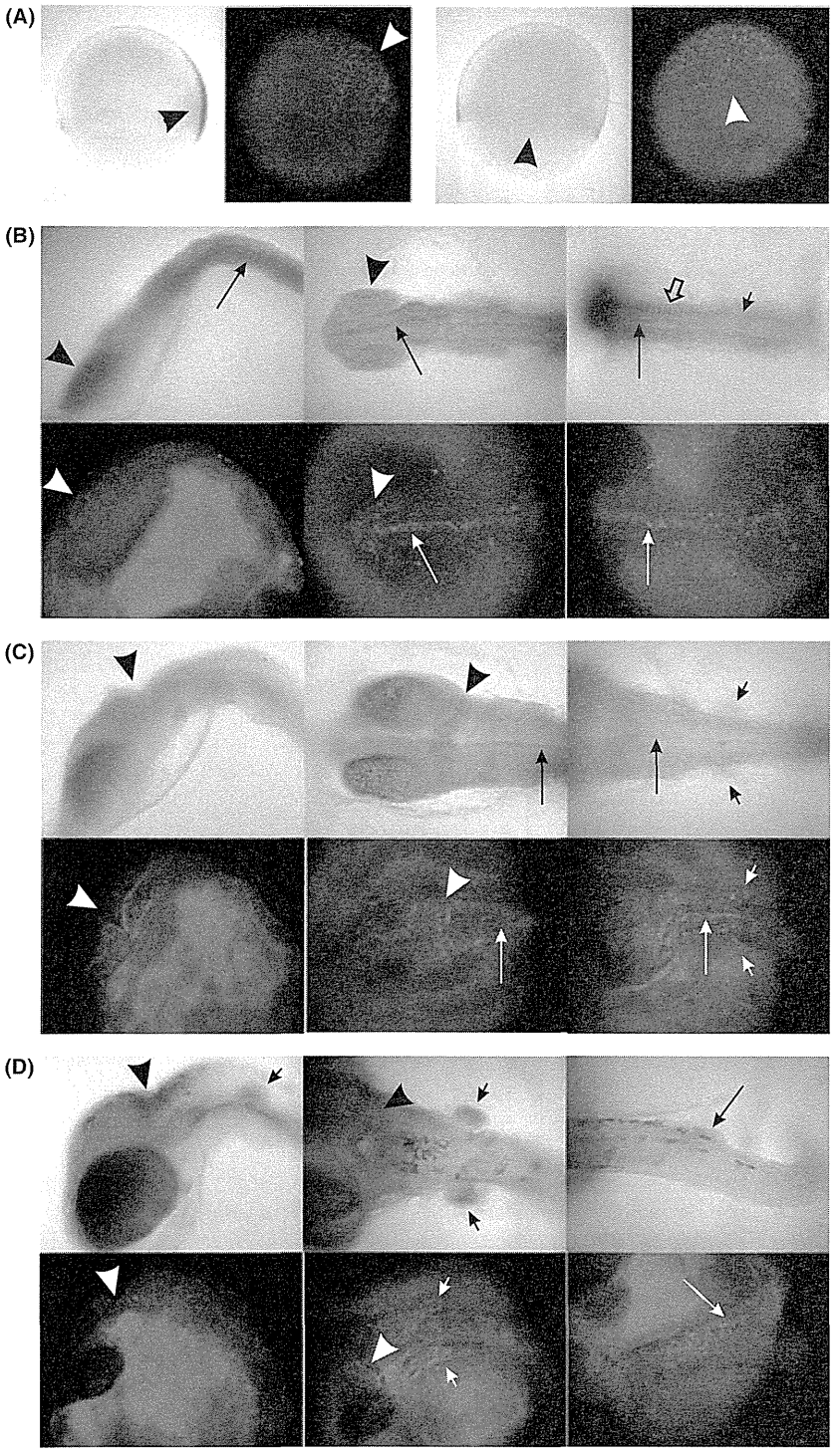

Fig. 1. *ESCO2* expression in medaka embryo. Whole-mount *in situ* hybridization analysis of *ESCO2* (micrograph) and immunohistochemical analysis of anti-phosphorylated histone H3 (M phase marker, fluorescence micrograph). (A) Gastrula stage (0.75 days postfertilization [dpf], stage 15). Left, lateral view; right, dorsal view; animal pole to top; arrowheads, embryonic shield. (B) Somitogenesis stage (1.0 dpf, stage 20). Left, lateral view; middle and right, dorsal view of head and tail, respectively; arrowheads, optic vesicles; long arrows, neural tube; open arrow, somite; short arrow, bilateral region in presomitogenic region. (C) Late somitogenesis stage (2.0 dpf, stage 28). Left, lateral view; middle and right, dorsal view of the head and pectoral regions, respectively; arrowheads, proliferative zone of optic tectum and prospective corpus cerebelli; long arrows, neural tube; short arrows, pectoral fin buds. (D) Gill blood vessel formation stage (3.0 dpf, stage 31). Left, lateral view; middle, dorsal view of the pectoral region; right, right dorsal view of abdomen; arrowheads, proliferative zone of optic tectum and prospective corpus cerebelli; short arrows, pectoral fin buds; long arrows, genital ridge.

performed immunohistochemical analysis of phosphorylated-histone H3, an M-phase marker. The immunopositive region was similar to the *ESCO2*-expressing region. These observations are in agreement with the fact that *ESCO2* is involved in cell division in other species (Skibbens *et al.* 1999; Hou & Zou 2005; Vega *et al.* 2005).

Developmental abnormalities in ESCO2 *mutant medaka*

In order to establish the RBS/SC model using medaka, we isolated mutant medaka from the TILLING library (Taniguchi *et al.* 2006). On sequence analysis, 18 mutations, including six missense, seven silent and five

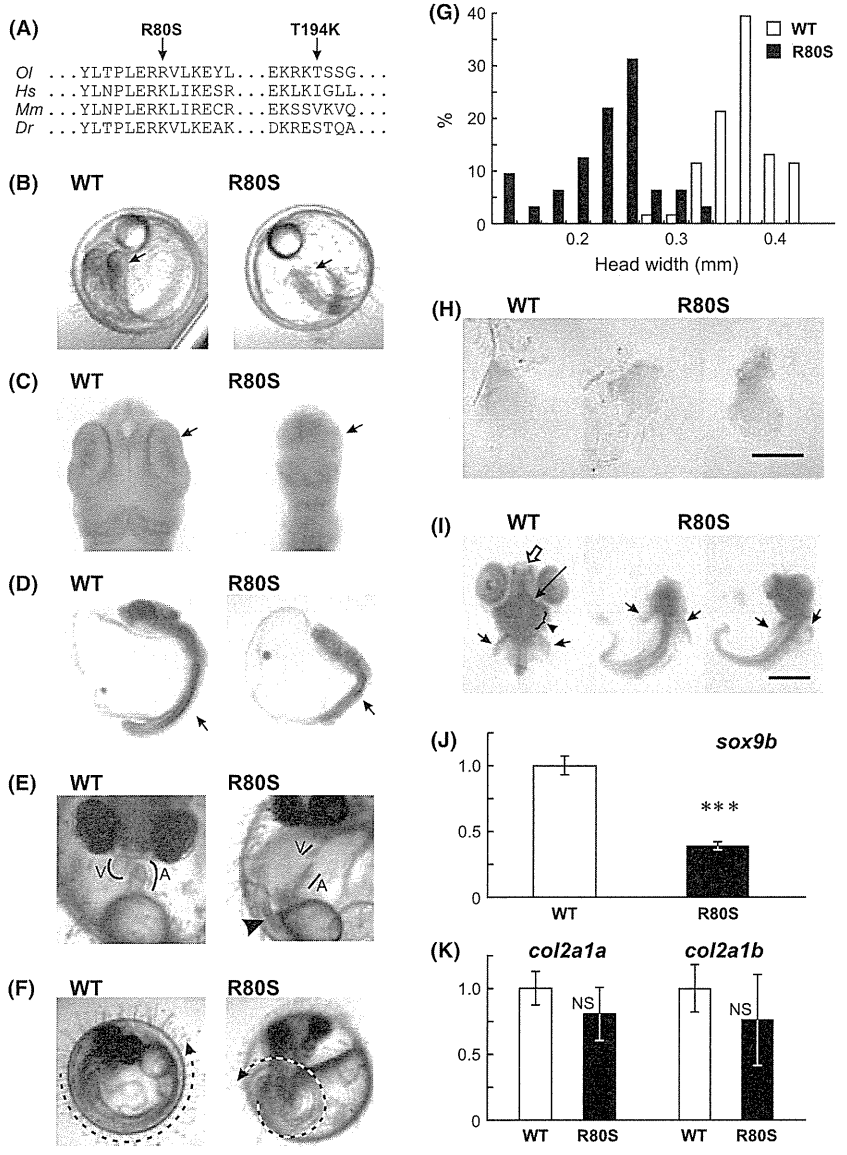

Fig. 2. Developmental abnormality of *ESCO2* mutant medaka. (A) Alignment of amino acid sequence of ESCO2 (R80 and T194 adjacent sequences). Note that R80 and adjacent region is conserved. *Ol*, *Oryzias latipes*; *Hs*, *Homo sapiens*; *Mm*, *Mus musculus*; *Dr*, *Danio rerio*. (B–C) Head deformity of R80S homozygous mutant (B, 2.5 days postfertilization [dpf] optical observation; C, 2.0 dpf whole-mount *in situ* hybridization [WISH] with *β-actin* probe). Note: small head and lack of eyes (arrows). (D) Somite malformation of R80S mutant (2.0 dpf WISH with *β-actin* probe). The number of somites was decreased and disarranged (arrows). (E) Heart malformation of R80S mutant (5.0 dpf). In mutant, defects in looping of heart and stagnation in the tail (an arrowhead) were observed. V, ventricle; A, atrium. (F) Body axis abnormality in R80S mutant (5.0 dpf). Dashed lines indicate body axis. (G) The head width of wild-type (WT) and R80S mutant (2.0 dpf). R80S mutants were significantly smaller than WT embryos ($P < 0.001$, $n = 32–61$). (H) Alcian blue staining of pectoral fin of WT and R80S mutant (6.0 dpf). Scale bar, 0.25 mm. In R80S mutants, the development of pectoral fins was normal (middle) or delayed (right). (I) Alcian blue staining of WT (head and pectoral region) and R80S mutant (whole body) (6.0 dpf, ventral view). In R80S mutant, defect of cartilage formation was observed. Open arrow, Meckel's cartilage; long arrow, ceratohyal; short arrow, pectoral fin; arrowheads, ceratobranchial arch. Scale bar, 0.5 mm. (J–K) *sox9b*, *col2a1a* and *col2a1b* expression in WT and R80S mutant (2.0 dpf) ($n = 13–14$). ***$P < 0.01$; NS, not significant; Student's *t*-test.

intronic *ESCO2* mutations were identified from 5760 clones. Among the six missense mutations, we selected R80S (240G→T, nucleotide) and T194K (581C→A, nucleotide) mutations for artificial insemination because R80 was highly conserved among species and T194K substitution confers the charged amino acid (Fig. 2A). Heterozygous (*ESCO2*$^{R80S/WT}$ and *ESCO2*$^{T194K/WT}$) embryos developed normally and did

Table 1. Genotyping and phenotype of *ESCO2* mutation[†]

Generation	*n*	*WT/WT* (%)	*R80S/WT* (%)	*R80S/R80S* (%)	Phenotype in R80S homozygous mutant (%)			
					Apparently normal	Developmental arrest[‡]	Cardiac abnormality	Body axis abnormality
F3[§]	73	30.1	53.4	16.4	100.0	0.0	0.0	0.0
F4[¶]	206	28.2	47.6	24.3	4.0	60.0	0.0	0.0
F5[††]	198	19.7	56.4	24.2	0.8	60.4	16.7	20.8

[†]Embryos and adults were progenies of heterozygous parents in all generations examined. [‡]Developmental arrest with craniofacial abnormalities and somite malformation by 2.0 days post fertilization (dpf). [§]Data of adults only. Embryonic development was not examined. [¶]F4 embryos (at stage 28, 2.0 dpf). [††]F5 embryos (by hatch). Sampling was carried out at appearance of abnormality. Cumulative value is shown.

not show pathological phenotypes. However, when the heterozygotes were intercrossed, the resulting *ESCO2*$^{R80S/R80S}$ homozygous mutants exhibited developmental delay and died before hatching. Homozygous *ESCO2*$^{T194K/T194K}$ embryos developed normally. Therefore, we further analyzed the R80S homozygous mutants in detail. Genotyping F3–F5 generation of backcrossed mutants (n = 73–206) showed that this mutation was transmitted in a Mendelian fashion (Table 1). The mutants developed normally during gastrulation and neurulation. From 1.5 dpf (stage 19), 60% of the mutants began to exhibit developmental delay. By 2.0 dpf (stage 28), their development was arrested (Table 1) and they were smaller than WT (Figs. 2G, S5A). The mutants showed head deformities (particularly brain and eye malformation, Fig. 2B,C) and somite malformation (Fig. 2D), both of which expressed *ESCO2* during the somitogenesis stages (Fig. 1). The rest of homozygous mutants developed normally until 2 dpf (hereafter called "escapers"). However they exhibited the heart abnormality (looping defect), stagnation (16.7% of mutants, Fig. 2E) and body axis malformation (20.8%, Fig. 2F) subsequently, and 91.7% of F5 mutants died by hatching period (Table 1), indicating that the homozygous mutation causes embryonic lethality. Because phocomelia and craniofacial abnormality are characterized in RBS/SC, we observed cartilage of mutants. The mutants were deficient in clear structure of cartilage. However, the pectoral fins were normally developed by 6.0 dpf in most mutants (Fig. 2H, middle). Some mutants showed developmental delay (Fig. 2H, right). The ventral cartilage elements of heads were almost defective in mutants by 6.0 dpf (Fig. 2I). Furthermore, the gene expression of *sox9b*, a transcriptional factor for cartilage formation, and *col2a1a* and *col2a1b*, components of cartilage, was examined at 2.0 dpf embryos. In mutants, *sox9b* was suppressed (Fig. 2J) but both *col2a1a* and *b* were not (Fig. 2K). At 2.0 dpf, the cartilage was not observed even in WT embryos (data not shown). Because the expression levels of *col2a1a* and *b* were very low, no significant difference between mutants and WT embryos may be observed.

It is known that ECO1 is essential for cellular viability in yeast (Skibbens *et al.* 1999). Although there are two related molecules in vertebrates, ESCO1 and ESCO2, each plays a distinct role and both are required for normal cell cycle progression (Hou & Zou 2005). To investigate the reason the homozygous mutants developed normally up to 1.5 dpf, we examined the effect of maternal mRNA accumulated in oocytes. To address this, we examined expression alleles using point mutation and polymorphism of *ESCO2* (Fig. S3). Until stage 14, *ESCO2* mRNA was derived from two maternal alleles. The paternal or embryonic *ESCO2* mRNA began to be expressed from stage 12, in agreement with the previous finding that midblastula transition of medaka begins at stage 11 (Aizawa *et al.* 2003). These data suggest that maternal mRNA of *ESCO2* caused normal development in R80S homozygous mutants during the early stages of development.

We attempted the rescue experiment by injection of WT *ESCO2* mRNA into mutant embryos. Unfortunately, we produced no detectable effects on phenotypes of mutants.

Almost all the mutations reported so far in RBS/SC patients are protein-truncating mutations (Schüle *et al.* 2005; Vega *et al.* 2005, 2010; Gordillo *et al.* 2008). Because the mutant we recovered from the TILLING library was the missense mutation, we constructed three morpholinos (Fig. S4), ATG mo (translation inhibitor), E2I2 mo (splicing inhibitor) and 5mis mo (control), and injected them into eggs immediately after fertilization to further investigate the role of ESCO2 in the embryogenesis. Because the maternal mRNA of *ESCO2* was accumulated until stage 14 as mentioned above, ATG mo was aimed at inhibiting both maternal and embryonic *ESCO2*, and E2I2 mo at inhibiting only embryonic *ESCO2*. The morpholinos had weak effect. Head deformities and somite malformation were not

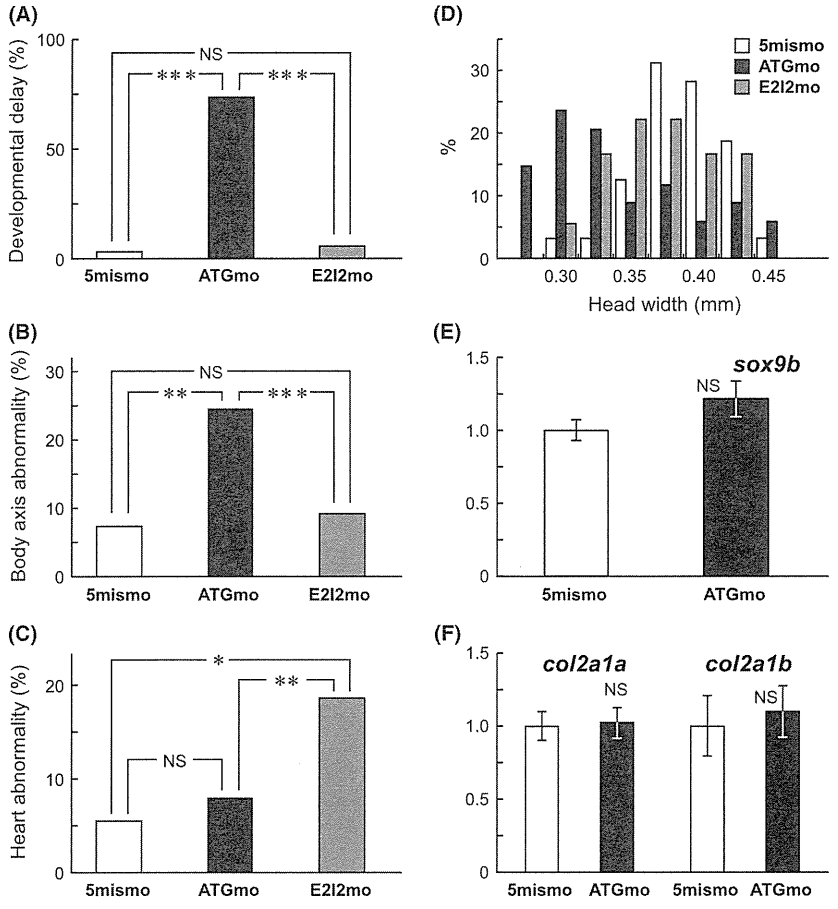

Fig. 3. Developmental abnormality of *ESCO2*-knockdown morphant. (A–D) The incidence of developmental delay (A), body axis abnormality (B, as in Fig. 2F) and heart malformation (C, as in Fig. 2E), and the head width (D) of morphants with 300 nmol/L of ATG mo (translation inhibitor, solid bars), E2I2 mo (splicing inhibitor, shaded bars) and 5mis mo (control, empty bars) injected just after fertilization. The 2.0-days postfertilization (dpf) embryos without heart beats were regarded as developmentally delayed. ATG mo morphants exhibited developmental delay. Body axis abnormality and heart malformation were observed by 5 dpf (n = 54–101). ATG mo morphants showed body axis abnormality. E2I2 mo induced heart malformation, but ATGmo did not. ***P < 0.001; **P < 0.01; *P < 0.05; NS, not significant; Tukey-type multiple comparison test (A–C); Tukey–Kramer test (D). ATG mo-injected morphants (2.0 dpf) were significantly smaller than control and E2I2 mo morphants (P < 0.001, n = 18–34). (E–F) *sox9b*, *col2a1a* and *col2a1b* expression in control and ATG mo morphants (2.0 dpf). NS, not significant; Student's t-test (n = 13).

obvious in morphants (data not shown). The expression of *sox9b*, *col2a1a* and *col2a1b* was not also affected in ATG mo morphants (Fig. 3E,F). This was in agreement with morphants not exhibiting head deformity. On the other hand, the ATG mo morphants exhibited a significantly higher incidence of developmental delay (Fig. 3A) and were significantly smaller in size (Figs 3D, S5B) compared to the control and E2I2 mo morphants at 2 dpf. The ATG mo morphants also exhibited significantly higher incidence of body axis abnormality than the control or E2I2 mo morphants (Fig. 3B). The incidence of heart abnormality was similar between the ATG mo morphants and control, but was threefold higher in E2I2 mo morphants compared to the control (Fig. 3C), suggesting that the phenotypes observed in R80S homozygous mutant fish are due to the loss-of-function effect of ESCO2. The phenotypes of ATG mo morphants and E2I2 mo morphants were different. The maternal and embryonic *ESCO2* are targets of ATG mo, and E2I2 mo may inhibit *ESCO2* after midblastula transition. Therefore, the difference of phenotype is attributable to the difference of timing for inhibition. Lastly, we crossed mutants (F4) of the original strain from the southern population, K-Cab, with another strain from the northern population, K-Kaga. The homozygous mutants (*ESCO2*$^{R80S/R80S}$) of the offspring (F′2) showed similar head deformities and developmental arrest by 2 dpf. Taken together, these results

demonstrate that R80S mutation is a loss-of-function mutation and is responsible for the developmental abnormality and the embryonic death.

Cytological abnormality in ESCO2 *mutant medaka*

Premature centromere separation (PCS) is caused by loss of ESCO2 and is diagnostic of RBS/SC (Schüle *et al.* 2005; Vega *et al.* 2005, 2010; Gordillo *et al.* 2008). To examine whether PCS is observed in R80S mutant medaka, we performed chromosomal analysis of 2-dpf embryos. Mutants showed a significant increase in the chromosomal abnormalities, including aneuploidy, chromosomal hyper-condensation and PCS (Fig. 4A, Table 2). Particularly, chromosomal hyper-condensation and PCS were observed in 39.6% and 6.6% of mutant cells, but only in 4.5% and 0.1% of WT, respectively. Thus, chromosomal abnormalities were observed in mutants similar to that in the *Eco1* mutant of yeast (Skibbens *et al.* 1999), with knocking down of *ESCO2* of HeLa cells (Hou & Zou 2005) and RBS/SC (Vega *et al.* 2005). The chromosomal hyper-condensation may be due to high sensitivity to colchicine in R80S mutants.

We monitored cells in the S-phase (Fig. 4B) and M-phase (Fig. 4C) with BrdU incorporation and an antibody to phosphorylated histone H3, respectively. Morphological differences between WT and mutant embryos were evident in the proliferative zone of the optic tectum, prospective corpus cerebelli, rhombic lips, pectoral fin buds and neural tube. In WT embryos, the proliferative cells were distinguishable and arranged in order. In contrast, the proliferative cells of mutants were widely distributed and out of order. The number of cells in the S- and M-phase tended to be slightly increased in mutants compared to WT embryos.

Next, we attempted cell cycle analysis by flow cytometry (Fig. 4D). In WT embryos, nuclei peaked at 2N DNA (corresponding to cells in the G1-phase), while a small fraction of cells were distributed between 2N and 4N DNA (S-phase), and at 4N DNA (G2/M-phase). Only 9.5% of cells were in the sub-G1 proportion. In contrast, mutant nuclei showed a marked increase in the sub-G1 population (41.2%) at the expense of cells in the G1-phase. Although a clear aneuploidy peak and enrichment of S and G2/M cells were not observed, S and G2/M cells slightly increased in mutants. To confirm the existence of apoptotic cells, we performed a TUNEL assay. In mutant embryos, a large number of cells underwent apoptosis throughout the body, while only a limited number of cells were TUNEL-positive in WT embryos (Fig. 4E). These results suggest that the R80S mutation of ESCO2 induces various chromosomal abnormalities including PCS and aneuploidy during cell division, and that the resulting apoptosis may cause developmental delay and eventual embryonic lethality.

Reduction of marker gene expression in ESCO2 *mutant medaka*

Because R80S mutant embryos showed morphological abnormalities, we analyzed the expression patterns of several marker genes, namely, *bf1*, *foxA2*, *iro3*, *krox20*, *notch1a*, *otx1* and *pax6*, as neural development and notochord markers, and *lfng* and *myf5* as somite markers using whole-mount *in situ* hybridization. The gene expression of almost all markers was downregulated and delayed in R80S mutants (Figs 5, S6). The expression of *pax6*, for example, in the eyes, was reduced in mutant embryos compared to WT ones at 2.0 dpf (Fig. 5A). However, when *pax6* expression in 2.0-dpf mutants was compared to 1.0-dpf WT, no significant differences were observed in the zona limitans intrathalamica. Similarly, the gene expression levels of *bf1*, *foxA2*, *iro3* and *lfng* in mutants at 2.0 dpf were similar to those in WT embryos at 1.0 dpf (Fig. S6). The *otx1* and *krox20* expression in 2.0-dpf mutants were similar to 1.5-dpf WT embryos (Fig. S6). Thus, the differences in expression were attributable to developmental retardation in mutants. The expression of *myf5* in mutants resembled 1.0-dpf and 2.0-dpf WT embryos (Fig. 5B). In contrast, strong reduction in *notch1a* expression was observed in mutants at 2.0 dpf (Fig. 5C,D). Because *notch1a* was expressed in WT embryos at 1.0–2.0 dpf, we speculate that this downregulation was not attributable to developmental retardation.

To confirm *notch1a* suppression in mutants, we quantified *notch1a*, *notch1b* (neurogenic markers [Lawson *et al.* 2002], Fig. 6A), and *ascl1a* and *ascl1b* (proneural markers, downstream targets of *notch1a* and *notch1b* in zebrafish [Allende & Weinberg 1994], Fig. 6B) mRNA of 2.0-dpf embryos by quantitative RT–PCR (qRT–PCR). We examined the genotype of all embryos prior to qRT–PCR and classified them into two groups: with and without morphological changes. Forty percent of the homozygous mutants were morphologically normal at 2.0 dpf. The neurogenic marker genes related to *notch* were dramatically suppressed in mutants exhibiting morphological abnormalities (Fig. 6A,B). Namely, the expression of *notch1a*, *notch1b*, *ascl1a* and *ascl1b* in mutants was suppressed by 41%, 50%, 9% and 8%, respectively, compared to the WT embryos. In contrast, no suppression of *notch1b* was observed in the morphologically normal mutants, while all the other neurogenic

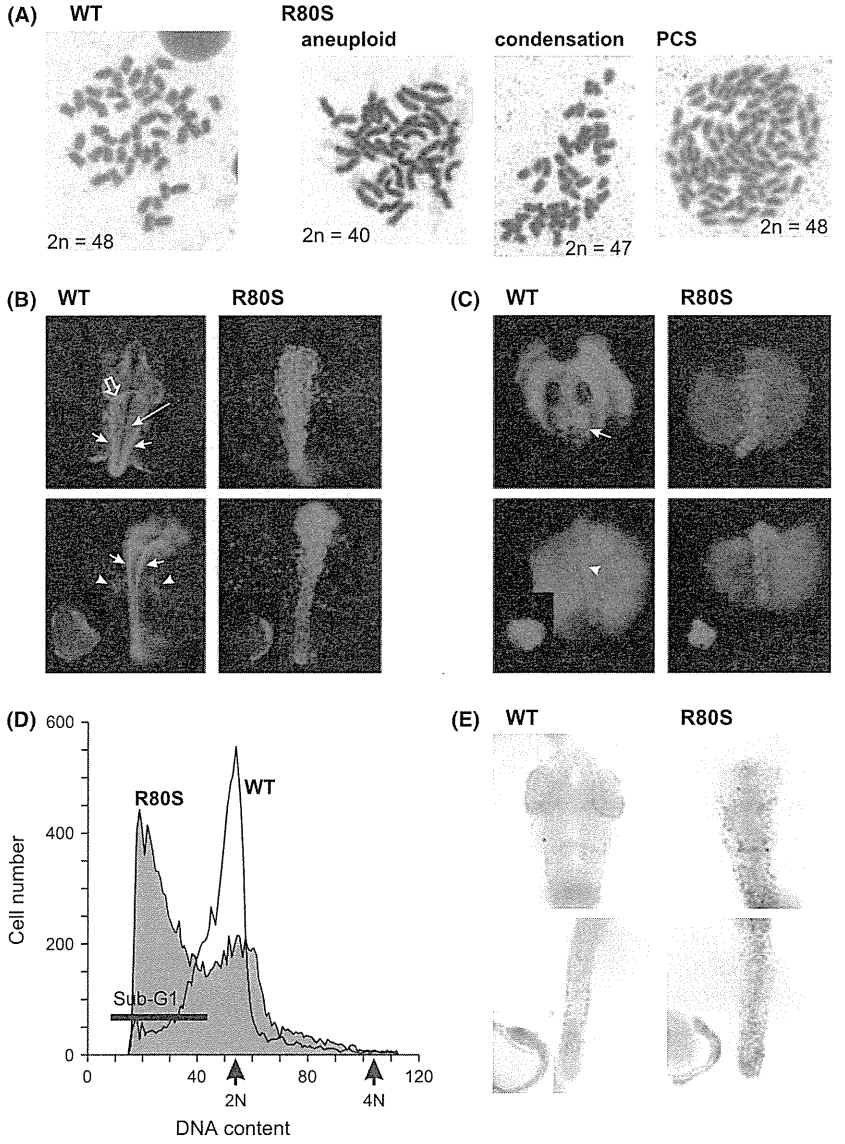

Fig. 4. Cytological abnormality of *ESCO2* mutant medaka. (A) Chromosomal analysis of wild-type (WT, leftmost) and R80S cells. Chromosomal preparation and Giemsa stain were applied to 2.0-days postfertilization (dpf) embryos. In R80S mutants, aneuploidy (shown as 2n = 40 versus 2n = 48 in WT), chromosomal hyper-condensation and premature centromere separation (PCS) were observed. (B) 5-bromodeoxyuridine (BrdU) labeling to detect cells in S-phase at 2.0 dpf. BrdU/Yamamoto solution (0.1%) was injected into the perivitelline space at 2.0 dpf. At 2 h after the injection, the embryos were fixed and immunohistochemically analyzed using anti-BrdU antibody. Top and bottom, dorsal view of the head and pectoral regions, respectively; inset in bottom panels, lateral view. BrdU labeling in the prospective corpus cerebelli (open arrow), rhombic lips (long arrow), the bilateral region of the midline (short arrows) and fin buds (arrowheads) was not detected in R80S mutants. (C) Anti-phosphorylated histone H3-labeling to detect cells in M-phase at 2.0 dpf. The embryos were fixed at 2.0 dpf and immunohistochemically analyzed by anti-phosphorylated histone H3 antibody. Top and bottom, dorsal view of the head and tail, respectively; inset of bottom panels, lateral view. The proliferating zone of the optic tectum and prospective corpus cerebelli (arrow) and the neural tube (arrowhead) was not immunoreactive in R80S mutant. (D) fluorescence-activated cell sorting (FACS) analysis of WT (open) and R80S (shaded) nuclei. The 2.0-dpf embryos were subjected to propidium iodide staining and FACS analysis. Note: the large proportion of R80S nuclei in sub-G1. (E) Terminal deoxynucleotidyl transferase-mediated dUTP nick end labeling assay indicates apoptotic cells throughout the whole body of R80S mutants. Top and bottom, dorsal view of the head and tail, respectively; inset of bottom panels, lateral view.

markers were suppressed by approximately 50% (Fig. 6A,B). We speculate that suppression of *notch1b* expression may be due to gross developmental defects and that the downregulation of *notch1a* is specific to *ESCO2* mutation regardless of developmental delay. Because *ascl1a* and *ascl1b* are downstream of

Table 2. Chromosomal analysis of medaka R80S mutants[†]

Genotype	*n*	Aneuploidy (%)	Hyper-condensation (%)	PCS (%)	String-like (%)
Embryos[‡]					
ESCO2$^{WT/WT}$	21	42.9	23.8	0.0	0.0
ESCO2$^{R80S/R80S}$	21	76.2*	71.4**	28.6**	19.0*
Cells					
ESCO2$^{WT/WT}$	941	6.2	4.5	0.1	0.1
ESCO2$^{R80S/R80S}$	182	25.3***	39.6***	6.6***	02.7***

*$P < 0.05$; **$P < 0.01$; ***$P < 0.001$, respectively (χ^2-test). [†]R80S embryos (F'2) were derived by crossing R80S (F4) heterozygous mutants of original strain with wild-type fish of another strain K-Kaga. The 2.0-days post fertilization (dpf) embryos were examined. [‡]Embryos with more than 10% of cells exhibiting abnormalities are regarded as abnormal embryos. PCS, premature centromere separation.

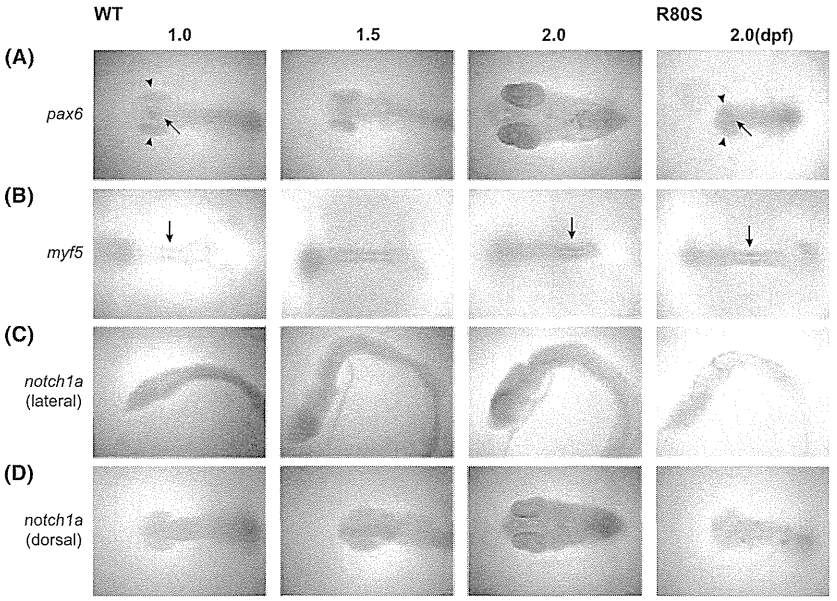

Fig. 5. Expression of marker gene in R80S (rightmost) and wild-type (WT) embryos. (A,B) Dorsal view of the *pax6* (A) and *myf5* (B) expression in the head and tail region, respectively. Expression of *pax6* in optic vesicles (arrowheads) is unclear in R80S mutant, but the expression in the zona limitans intrathalamica (arrows) is evident in both WT and R80S mutants. Expression of *myf5* (arrows) in R80S embryo resembles 1.0- and 2.0-day postfertilization (dpf) WT embryos. Lateral (C) and dorsal (D) view of the *notch1a* expression. Note: *notch1a* expression disappears in R80S mutant.

both *notch1a* and *notch1b*, the reduction of *ascl1a* and *ascl1b* may be more pronounced in morphologically abnormal mutants.

Next, we examined *GATA-1* and *notch3* (vascular differentiation markers in zebrafish [Lawson *et al.* 2001, 2002], Fig. 6C) because the heart was malformed in mutants. They were suppressed by 57% and 30%, respectively, in mutants with morphological abnormalities. In mutants with normal morphology, no significant reduction in *GATA-1* was observed (Fig. 6C), suggesting that *GATA-1* suppression may accompany general developmental delay, as is the case with *notch1b*. To confirm these data, we investigated the gene expression in morphants. We used the ATG mo and 5mis mo (as control), because ATG mo inhibits maternal and embryonic *ESCO2*. The ATG mo morphants showed suppression of *notch1a* (by 67%), *notch1b* (66%) and *notch3* (71%) (Fig. 6D,E). Downregulation of *notch1b* may be attributable to the developmental delay in ATG mo morphants (Fig. 3A). Thus, *ESCO2* mutation causes downregulation of *notch1a* and *notch3*. In summary, these data suggest that ESCO2 may play a role in embryogenesis through upregulation of critical genes such as *notch1a* and *notch3*.

Discussion

Establishment of RBS/SC model medaka

We established a medaka model of RBS/SC using the TILLING method and characterized it using a reverse